

# Structure and Properties of Bioinert Mo–Nb Coating Formed on Titanium Grade 5 Medical Alloy by Electroexplosive Method

D. A. Romanov<sup>a, \*</sup>, K. V. Sosnin<sup>a, \*\*</sup>, S. Yu. Pronin<sup>a, \*\*\*</sup>, V. V. Pochetukha<sup>a, \*\*\*\*</sup>,  
Yu. F. Ivanov<sup>b, \*\*\*\*\*</sup>, and V. E. Gromov<sup>a, \*\*\*\*\*</sup>

<sup>a</sup> Siberian State Industrial University, Novokuznetsk, 654006 Russia

<sup>b</sup> Institute of High Current Electronics, Siberian Branch, Russian Academy of Sciences, Tomsk, 634055 Russia

\*e-mail: romanov\_da@physics.sibsiu.ru

\*\*e-mail: K.sosnin@mail.ru

\*\*\*e-mail: Major-Pronin@mail.ru

\*\*\*\*e-mail: v.pochetuha@mail.ru

\*\*\*\*\*e-mail: yufi55@mail.ru

\*\*\*\*\*e-mail: gromov@physics.sibsiu.ru

Received November 1, 2022; revised February 4, 2023; accepted March 1, 2023

**Abstract**—An attempt was made to solve the problem of creating a coating for an implant having better biological compatibility than Titanium Grade 5 medical titanium alloy. A coating of Mo–Nb composition was prepared by the electroexplosive method on Titanium Grade 5 medical titanium alloy and formed as a result of the simultaneous electric explosion of foils made of molybdenum and niobium. A set of studies was carried out to determine the structure, phase composition, and properties of the prepared coatings. It is shown that the hardness of the coating surface layer is 60% and the Young's modulus is 43% higher than the corresponding characteristics of Titanium Grade 5 alloy. The thickness of the layer with high (relative to the substrate) values of hardness and Young's modulus reaches 80 μm. It was found that the coating wear parameter is 1.8-fold and the coating friction coefficient is 1.6-fold higher than the substrate wear parameter and friction coefficient. It was determined that, along with coating atoms, the surface layer comprises Al, Ti, V, O, and C atoms, indicating that the coating is doped with the substrate atoms. In the detected coating stratification by elemental composition, the top part of the coating is enriched in niobium atoms, and the bottom part is enriched in molybdenum atoms. The coating was shown to have a polycrystalline structure formed by a molybdenum-based solid solution. The bulk and the grain boundaries compose the second phase comprising α-Ti, Nb, Mo<sub>9</sub>Ti<sub>4</sub>, and NbTi<sub>4</sub> of various shapes and sizes. The phase composition studies revealed no vanadium or aluminum compounds, which reduce the biocompatibility of coatings. The detected phases comprise only molybdenum, niobium, and titanium, which are bioinert, which allows predicting higher biocompatibility compared to the that of Titanium Grade 5 medical alloy. It is recommended to use the resulting coatings for further clinical tests.

**Keywords:** Mo–Nb coating, electroexplosive method, structure, microhardness, wear resistance

**DOI:** 10.1134/S2075113324700163

## INTRODUCTION

The accelerating population aging is accompanied by a trend of rapid growth in the number of patients with orthopedic injuries and diseases. In this regard, the treatment of bone defects is becoming an increasingly acute clinical and social problem. Currently, fixation of bones with bioinert metal structures is a routine operation, which is provided for millions of people every year [1, 2]. Biomaterials play a key role in the success of modern dental and orthopedic operations [3]. Metals have been the main choice for biomedical implants for over a century [4]. Owing to their high tensile and compressive strength, high yield strength,

fatigue strength, ductility, hardness, and toughness, metals are widely used for orthopedic implants [5].

Currently, titanium alloys are widely used in implants, but with the increasing use of titanium implants, the number of their premature failures is also increasing. The main reason for implant failure is low osseointegration of bone tissue to the implant surface (weak connection between the implant and the surrounding bone tissue) [6]. For the Ti–6Al–4V alloy, a significant danger is posed by aluminum and vanadium ions released as a result of corrosion. Their carcinogenicity was confirmed by studies [7, 8].

To overcome the disadvantages of the Ti–6Al–4V alloy, its analogs have been developed from such non-

toxic elements as niobium, tantalum, zirconium, hafnium, and molybdenum [9]. Alloys of the Ti–Mo system have recently attracted particular interest [10–12]. A study [10] was carried out on the electrochemical behavior of pure Ti and Ti–Mo alloys containing 6 to 20 wt % Mo. Tests in a chlorine-containing solution showed active spontaneous growth of a passivating oxide film, which entails an increase in the corrosion resistance of the alloys in question. Similar results were obtained when studying alloys of the Ti–10Mo system [12].

The key factor influencing the reliable fixation of the implant and its further functioning is the ability of the material surface to create a strong connection to the surrounding bone tissue [13, 14]. Such properties of biomaterials as microstructural topography, surface chemistry, or surface energy/wettability influence the behavior of cells in contact with the implant and accelerate or retard their adhesion, proliferation, and migration [15], which ultimately determines the strength of the bond between the implant and surrounding bone tissue.

The antimicrobial properties of molybdenum [16, 17] and its trioxide [16, 18] were studied. Furthermore, the antibacterial effectiveness of MoO<sub>3</sub> nanoplates was demonstrated [16] against pathogenic bacteria *Escherichia coli*, *Salmonella typhimurium*, *Enterococcus faecalis*, and *Bacillus subtilis*, comparable to that of standard antibiotic kanamycin [19].

Niobium-based coatings also have a favorable effect on biocompatibility [20]. An in vitro study [21] demonstrated the viability of osteoblast-like cells (MG-63) on Ti–Nb system coatings.

In Russia, in the field of electroplasma coating of implant structures, there is a widely known work of V.N. Lyasnikov, who developed, patented, and introduced into manufacture and clinical practice a system of dental implants having no analogs in our country owing to a special multilayer bioactive coating applied using plasma sputtering [22]. Also noteworthy are the works of I.V. Rodionov and I.V. Perinskaia et al. [23, 24] concerning the research of bioinert and bioactive reinforcing coatings in the field of plasma coatings and additive technologies for ion alloying of metals used in implants.

A promising approach to applying coatings that meets all the above requirements may be the electroexplosive method, which essence is the electrical explosion of a conductor and the subsequent melting of the surface of the implant created by a plasma jet, which allows forming coatings that can work in the conditions of the human body [25, 26]. Thus, coatings based on titanium and zirconium were prepared by the electroexplosive method [25], and Ta10W coatings were prepared [26]. Therefore, it is necessary to develop new methods for producing coatings of a certain composition that meet the functioning requirements in the human body. For titanium implants, such

a coating may be a Mo–Nb coating formed by the electroexplosive method.

The goal of this work was to study the structure and properties of a Mo–Nb coating formed on Titanium Grade 5 medical alloy by the electric explosion method. To achieve the goal, the following problems were set and solved:

- (1) Preparing a Mo–Nb coating by the electroexplosive method.
- (2) Studying the mechanical properties (microhardness, Young's modulus, wear parameter under dry friction-sliding conditions, friction coefficient) of Mo–Nb coating.
- (3) Studying the structure of the Mo–Nb coating by scanning and transmission electron microscopy.
- (4) Drafting recommendations to submit the resulting coatings for clinical trials of a specific type of implant.

## MATERIALS AND METHODS

The test samples of Mo–Nb coatings were deposited on a substrate made of Titanium Grade 5 medical titanium alloy by the electroexplosive method. The coating thickness was 30 to 60 μm. The electroexplosive spraying used a two-layer foil comprising molybdenum (100 mg) and niobium (100 mg). The products of the electric explosion were fed through a titanium nozzle onto the substrate sample. The electric explosion provided an absorbed power density of 1.5 GW/m<sup>2</sup> on the processed material surface, a pressure of ~12.5 MPa in the shock-compressed layer near the irradiated surface, a residual gas pressure of ~100 Pa in the working chamber, and a plasma temperature of ~10<sup>4</sup> K at the exit of the silver nozzle, and a time of plasma exposure to the sample surface of 100 μs. The electroexplosive treatment was carried out using an EVU60/10M station. The substrate samples had the shape of plates with dimensions of 20 × 20 × 5 mm.

The coating structure and elemental and phase compositions were studied by scanning (SEM 515 Philips) and transmission diffraction electron (JEOL JEM-2100F, Japan) microscopy. The results were obtained by special computer programs: INCA Point & ID (for qualitative and quantitative elemental analysis) and Mapping and QuantMap (for mapping method). The elemental composition mapping analysis provides continuous X-ray data collection for all elements at each point in a given image area. The coating phase composition was determined by X-ray diffraction analysis using a Shimadzu XRD-6000 diffractometer. The recording was carried out with copper filtered CuK<sub>α1</sub> radiation and a CM-3121 monochromator. The phase composition was analyzed using the PDF 4+ databases, as well as the POWDER CELL 2.4 full-profile analysis program.

Microhardness was measured with a DUH-211S dynamic microhardness gage manufactured by Shi-

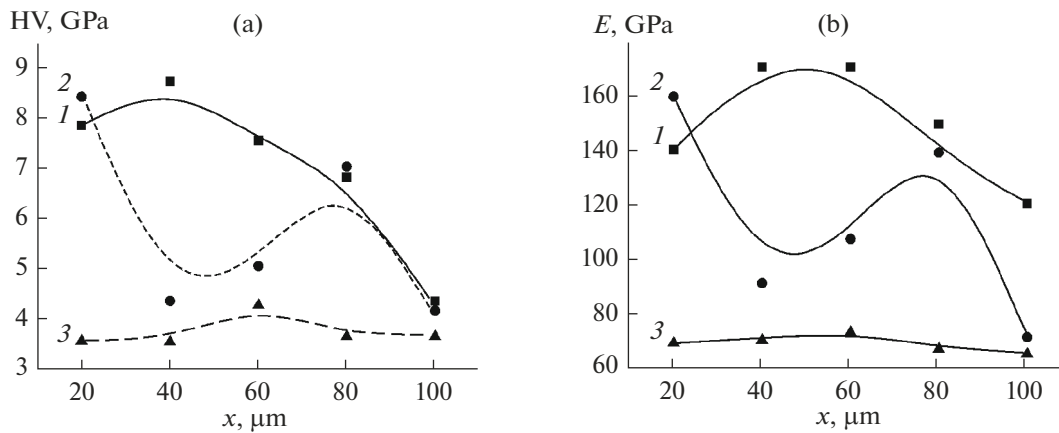


**Fig. 1.** Profiles of microhardness (a) and Young's modulus (b) of three cross-sectional tracks of the Mo–Nb coating formed by the electroexplosive method: (1–3) three parallel tracks randomly selected for measurement.

madzu (Japan) at a load of 100 mN on transverse sections along three tracks consisting of five indenter prints and located at distances of 20, 40, 60, 80, and 100  $\mu\text{m}$  from the coating surface. The distance between tracks was 50  $\mu\text{m}$ . Young's modulus was simultaneously measured with the same instrument as the microhardness. The tribological properties were characterized by the wear resistance and friction coefficient (TRIBOTester Pin on Disc and Oscillating tribometer manufactured by TRIBOtechnic, France), which were determined in the test conditions of alumina ball with a diameter of 6 mm as counterbody, wear track diameter of 4 mm, load of 10 H, sample rotation speed of 25 mm/s, and friction path length of 50 m (dry friction conditions at room temperature).

## RESULTS AND DISCUSSION

### Investigation of Microhardness and Young's Modulus

Figure 1 shows the microhardness and Young's modulus profiles of a Mo–Nb coating prepared on Titanium Grade 5 alloy by the electroexplosive method.

The microhardness profile from 3.6 to 8.5 GPa for three parallel tracks (Fig. 1a), especially in the surface layer of different coating sections, showed a significant nonuniformity. Similar results were observed when plotting the Young's modulus profile (Fig. 1b). Obviously, these facts indicate the nonuniform coating structure formed by the electroexplosive method.

The averaged profiles of microhardness and Young's modulus for three tracks allowed distinguishing a hardened surface layer 30  $\mu\text{m}$  deep from the coating surface (layer I), an intermediate layer 60  $\mu\text{m}$  thick (layer II) with constant slightly lower values of microhardness and Young's modulus, and a transition layer 10  $\mu\text{m}$  thick (layer III) with rapidly decreasing characteristics (Fig. 2). The thickness of the layer with high (relative to the substrate) hardness values reaches 80  $\mu\text{m}$ .

### Investigation of the Wear Parameter under Dry Friction-Sliding Conditions and the Friction Coefficient

The tribological tests have shown that the wear parameter of the coating surface layer is  $9.7 \times 10^{-4} \text{ mm}^3/(\text{N m})$ ,

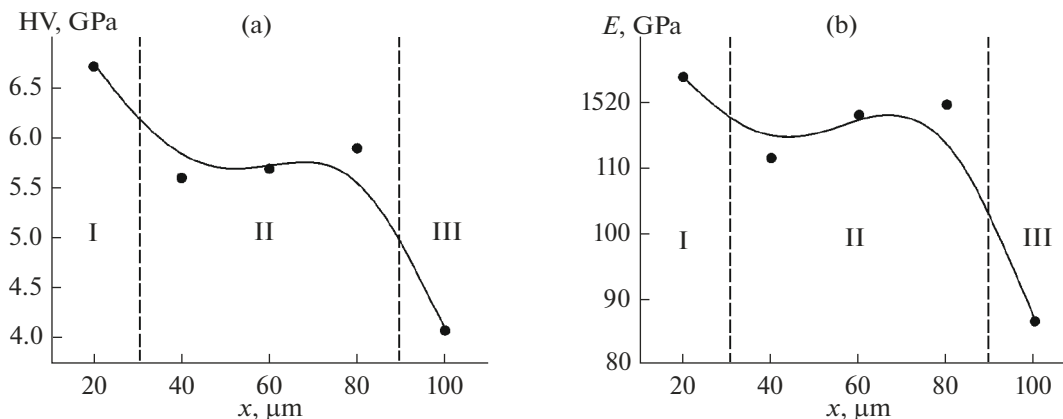


**Fig. 2.** Profiles of microhardness (a) and Young's modulus (b) averaged according to the results of the study of three tracks of transverse sections of the Mo–Nb coating formed by the electroexplosion method.

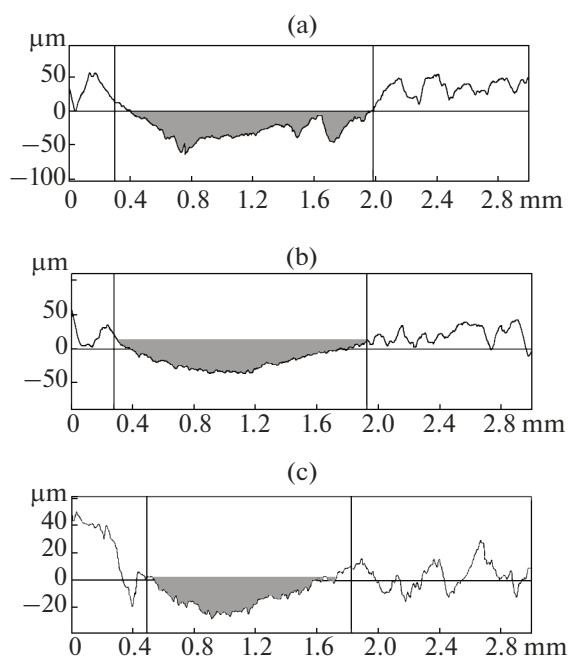


**Fig. 3.** Profiles of the friction track in various sections of the Mo–Nb electroexplosive coating.

which is 1.8-fold greater than the substrate wear parameter of  $5.4 \times 10^{-4} \text{ mm}^3/(\text{N m})$ . The coating friction coefficient ( $\mu = 0.69$ ) is 1.6-fold higher than the substrate friction coefficient  $\mu = 0.43$ ; therefore, the tribological characteristics of the coating are inferior to those of the substrate. Noteworthy are the profiles of the friction tracks, indicating the nonuniform coating structure (Fig. 3).

The profiles in Fig. 4 show that, firstly, the running-in stage of the coated sample is significantly longer than that of the Titanium Grade 5 alloy, and, secondly, the friction force of the coated sample is signifi-

cantly (1.4-fold) higher than that of the unmodified substrates. The latter may indicate a change in the coating friction mechanism from adhesive (at the initial stage of testing) to abrasive [27]. Consequently, the tribological characteristics of the coating are inferior to those of the substrate; that is, the combination of a high wear parameter and a high friction coefficient will ensure a gentle effect of the implant on bone tissue (bone will not be destroyed during operation). And the high friction coefficient of the Mo–Nb coating will ensure good primary fixation of the implant in the bone tissue.

### Investigation of Coating Structure

Figure 5 presents the results demonstrating the coating surface structure (Fig. 5a) as well as the elemental composition and distribution of elements of the surface layer (Figs. 5b–5f). It is clearly visible that, in the surface layer, along with Mo and Nb coating atoms, there are Al, V, and Ti atoms, which indicates the mutual diffusion of coating and substrate elements, that is, a cohesive (metallurgical) bond between the coating and the substrate. Vanadium and aluminum are present on the surface of the coating in significantly smaller quantities compared to the substrate. This fact clearly indicates that the biocompatibility of the resulting coatings should be higher compared to Titanium Grade 5 alloy.

Figure 6 and Table 1 show the results of quantitative elemental analysis of the coating surface layer.

The results in Table 1 were analyzed to show that the coating surface layer comprises, firstly, impurity oxygen and carbon atoms in large quantities; secondly, substrate atoms (Al, V, Ti); and thirdly, nonuniform distribution of atoms forming the coating.

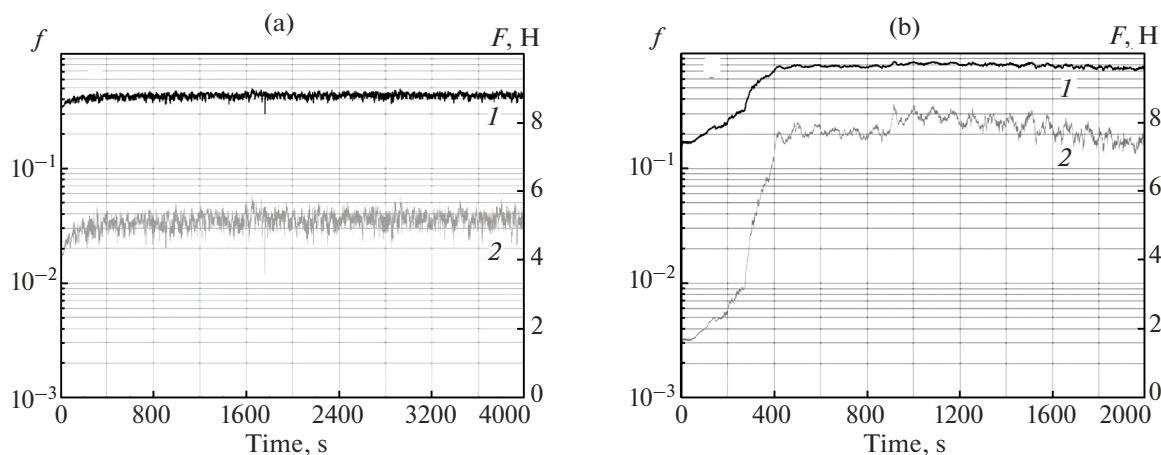


**Fig. 4.** Time dependence of the friction coefficient (curve 1) and friction force (curve 2) in tribological tests of Titanium Grade 5 medical alloy (a) and Mo–Nb electroexplosive coating on Titanium Grade 5 medical alloy (b).

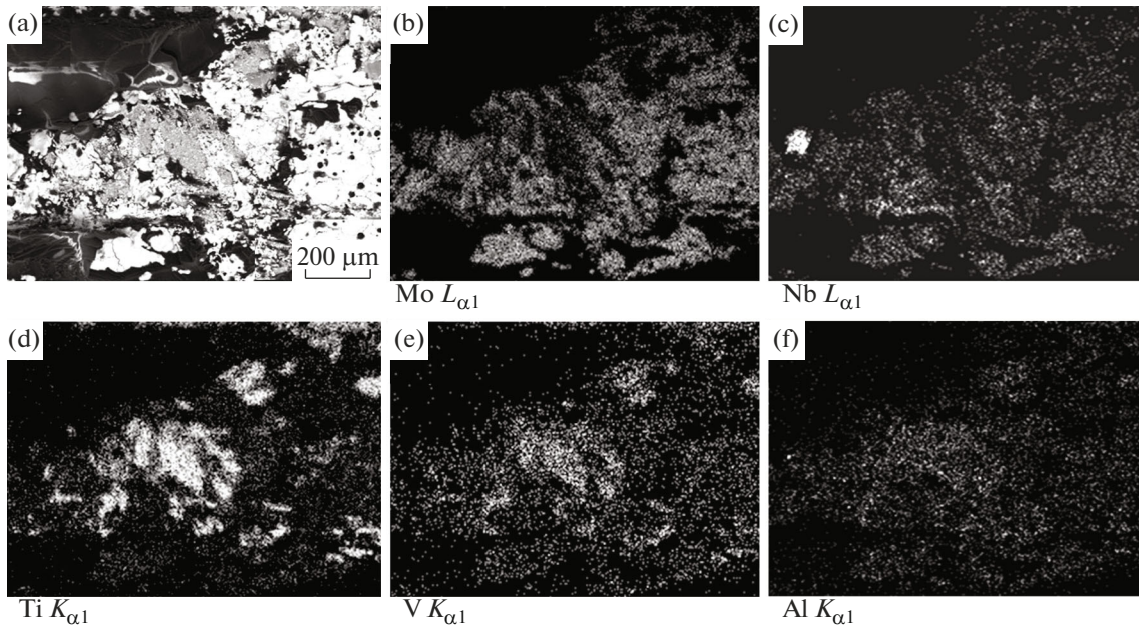


Fig. 5. Electron microscopic image of the coating surface structure (a) and analysis of the distribution of chemical elements in the coating (b–f).

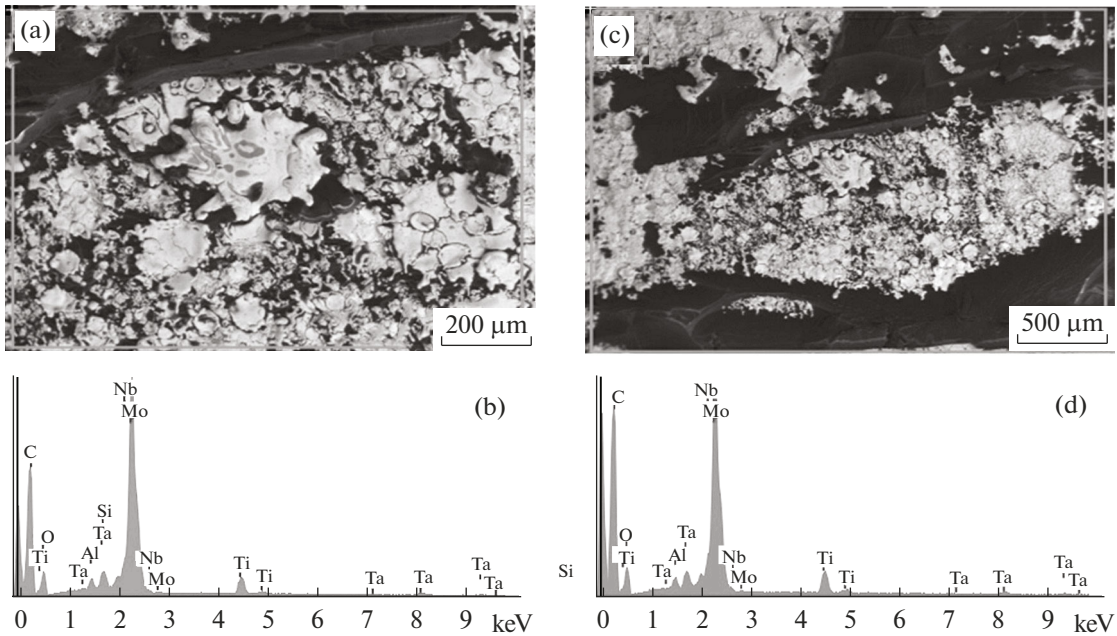


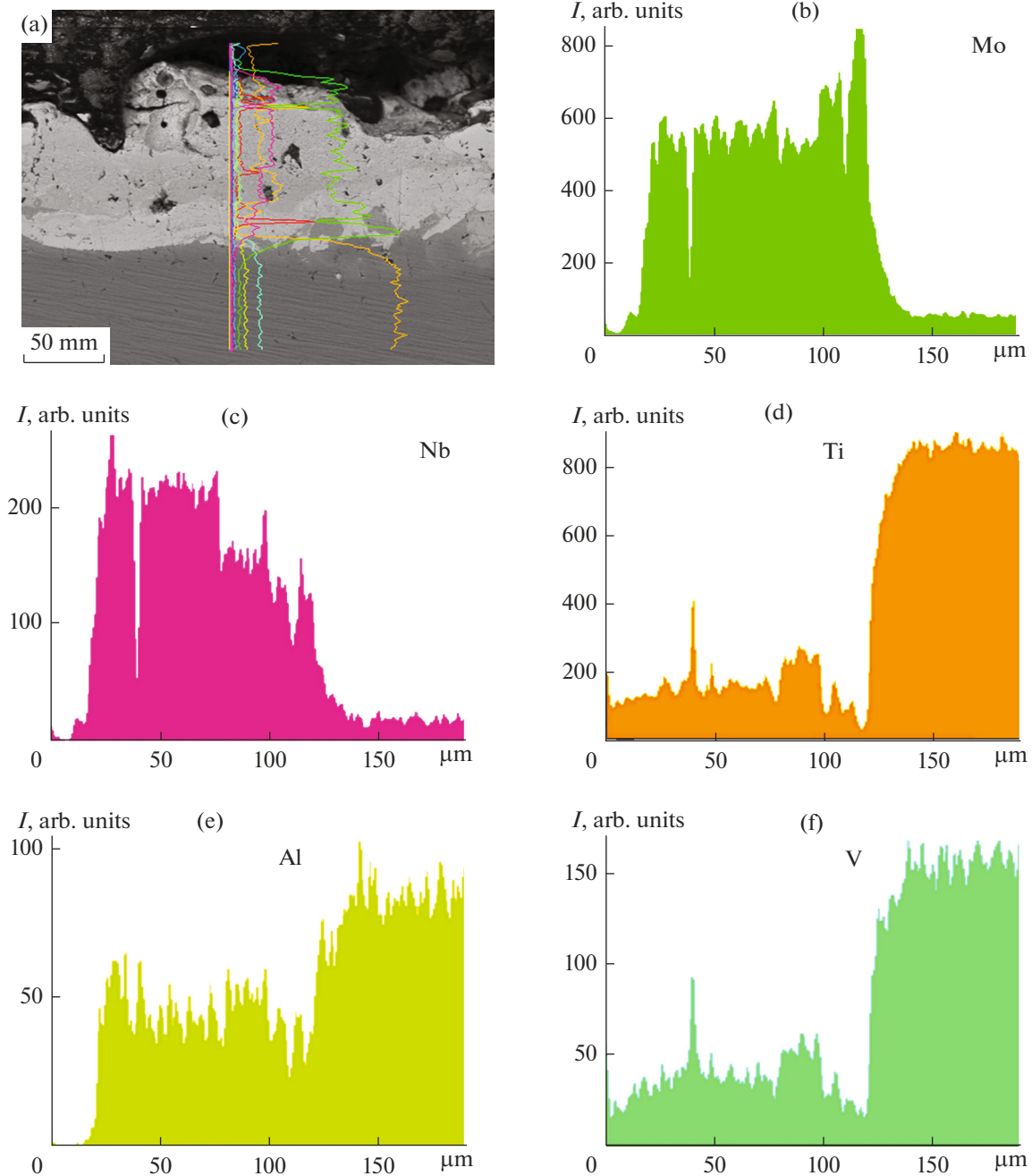
Fig. 6. Electron microscopic image of the coating surface structure (a, b) and energy spectra corresponding to these areas (c, d).

Table 1. Results of X-ray microspectral analysis of the areas of the surface layer of the coating presented in Fig. 6

Test area, Fig. 6	Element, wt %							
	C	O	Al	Si	Ti	Nb	Mo	Ta
a	56.66	13.06	0.44	0.34	1.92	1.90	24.49	1.19
b	61.1	12.54	0.37	0.0	2.1	1.96	20.38	1.55

**Table 2.** Results of X-ray microanalysis of various sections of the transverse section of the coating

Spectrum	Element, wt %								
	O	Al	Si	Ti	V	Cr	Nb	Mo	Ta
1	6.04	1.23	0.84	15.57	1.01	1.03	11.1	61.5	1.97
2	2.95	0.94	0.58	11.51	0.56	0.41	17.36	63.75	1.95
3	7.68	0.84	0.73	7.99	0.0	0.4	20.22	59.34	7.8

**Fig. 7.** Electron microscopic image of the coating cross section (a) and results of analysis of the elemental composition of the coating (b–f).

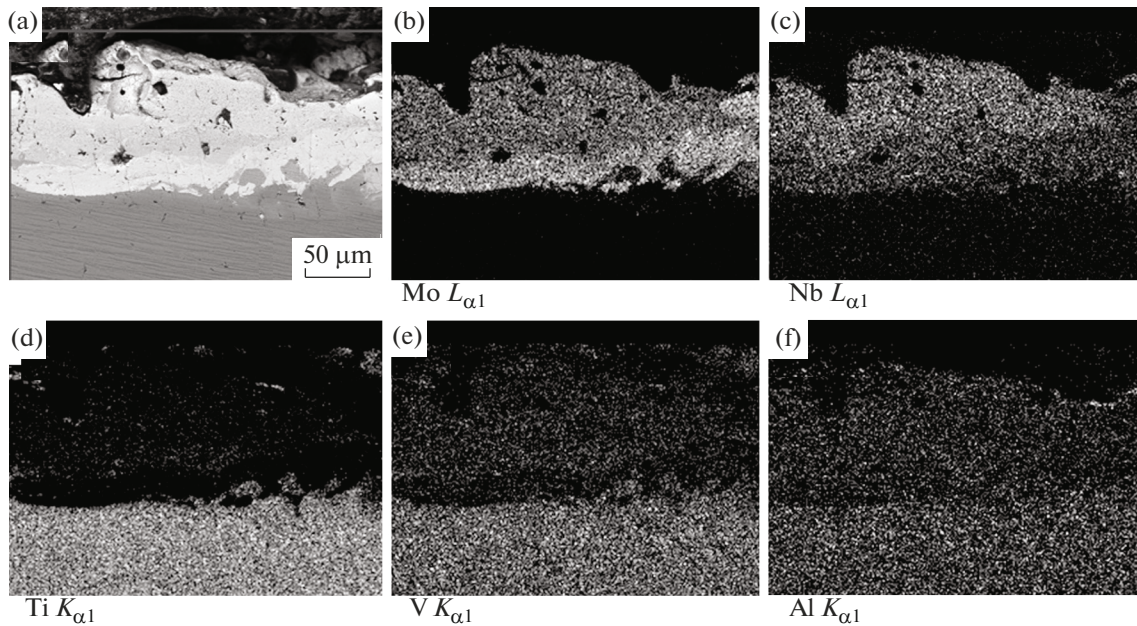


**Fig. 8.** Distribution of chemical elements in the system of the coating (Mo–Nb) and substrate (Titanium Grade 5 medical alloy) obtained by the mapping method.

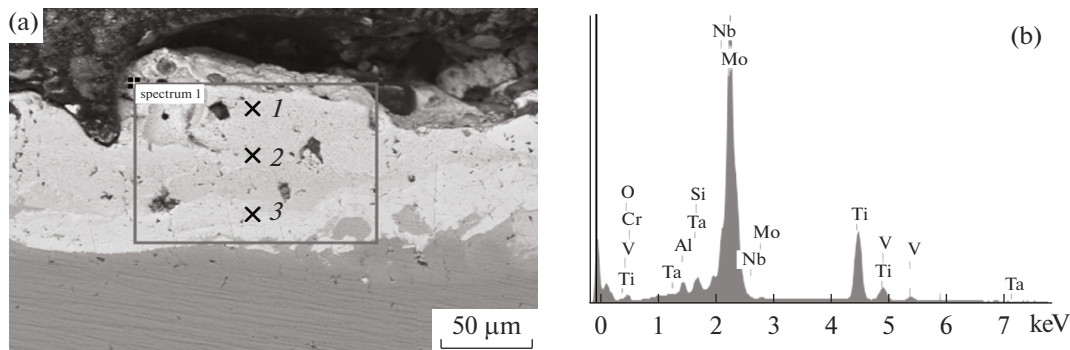


**Fig. 9.** SEM image of the cross section of the coating (a) and near the interface with the substrate (b) according to the areas of the set of spectra 1–3 with the elemental composition presented in Table 2.

A study of the coating cross section of the (Fig. 7) demonstrates a change in the elemental composition of the coating along its thickness. As one would expect, the coating is based on molybdenum and niobium. Titanium atoms are present in the coating in a slightly smaller quantity relative to niobium. Molybdenum and niobium atoms are distributed unevenly in the coating; there are areas enriched and depleted in Mo and Nb atoms. One can note an increase in the concentration of molybdenum and niobium atoms in the layer separating the coating and the substrate. In turn, the coating elements (Mo and Nb) penetrate into the substrate (Figs. 7a–7c). Figure 8 presents changes in the elemental composition of the coating and the adjacent substrate layer as determined by the cross-

sectional mapping method. The coating clearly shows a difference in the elemental composition: the bottom part of the coating is enriched in molybdenum atoms (Fig. 8b), and the top part is enriched in niobium atoms (Fig. 8c).

So, Fig. 8b obtained in the characteristic X-ray radiation of molybdenum atoms shows a brighter contrast (higher intensity of X-ray radiation of atoms, higher concentration) at the bottom part of the coating, thus indicating a higher concentration of molybdenum atoms in the bottom part of the coating, and Fig. 8c shows a brighter contrast in the top part of the coating, thus indicating a higher concentration of niobium atoms in this part of the coating. Thus, separa-

**Table 3.** Results of quantitative elemental analysis of the surface layer of the Mo–Nb coating

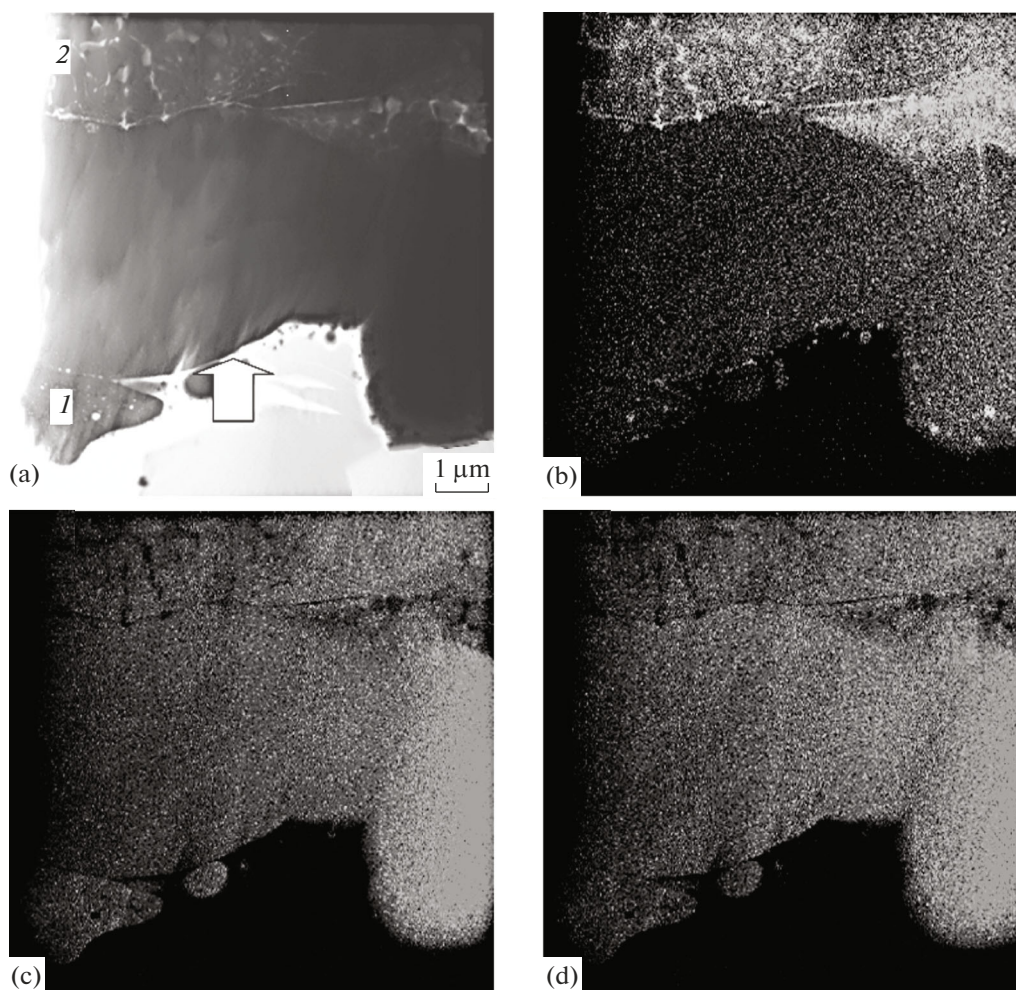
Element	Energy, $E$ , keV	Content		Number of pulses when signal is collected from atoms of given element	Error, %
		wt %	at %		
Ti ( $K$ )	4.508	15.19	26.20	183 318.52	0.02
Nb ( $L$ )	2.166	28.07	24.95	118 213.63	0.04
Mo ( $L$ )	2.293	56.74	48.85	219 576.42	0.02
Total	–	100	100	–	–

tion of molybdenum and niobium in the formed coating is observed.

Figure 9 and Table 2 show the results of a quantitative elemental analysis of the coating performed when studying the structure of a transverse section to confirm the above data (Fig. 5).

Figure 10 shows the results of the phase composition studied by X-ray diffraction analysis, transmis-

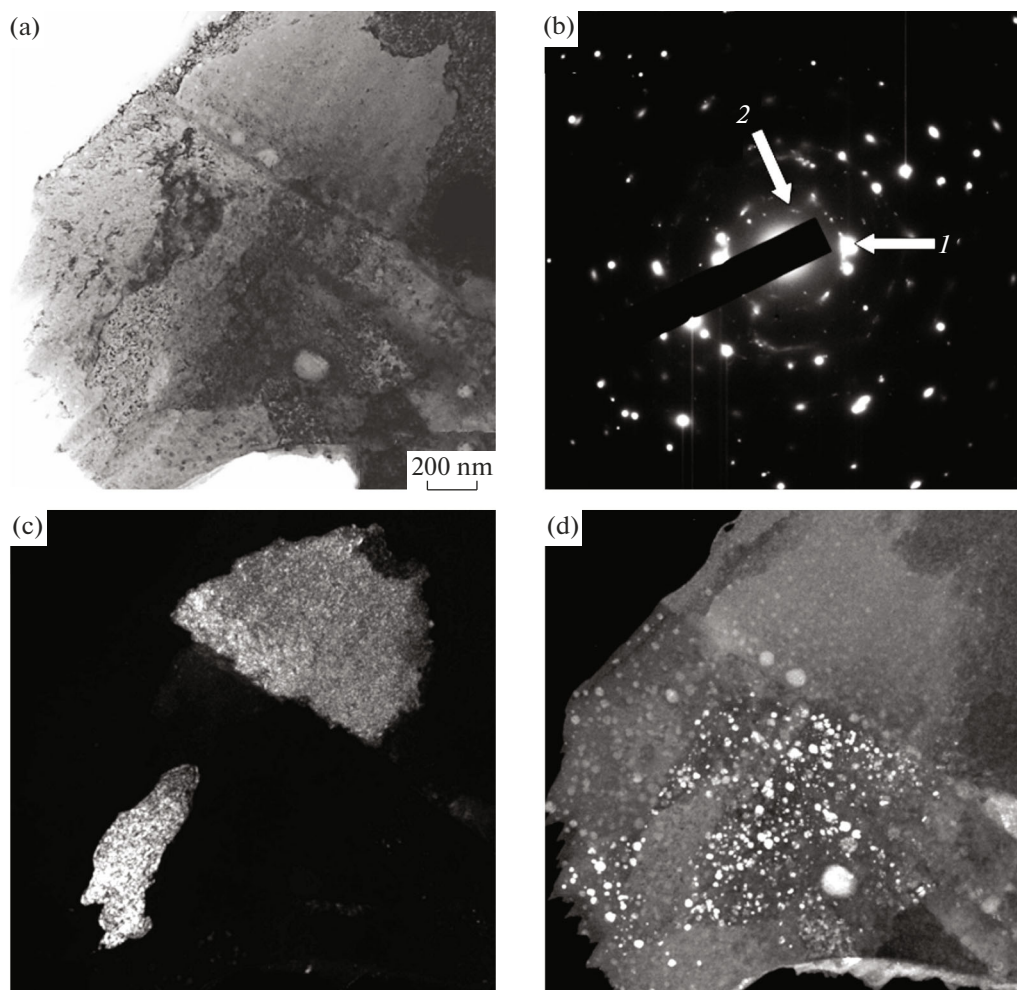
sion electron microscopy, and electron diffraction. Figure 10a shows an electron microscopic image of the coating surface structure layer about 9  $\mu\text{m}$  thick. It is clearly seen that the main chemical elements of this layer are also molybdenum and niobium (Figs. 10c and 10d). An additional element of the coating surface layer is titanium as the major chemical element of Titanium Grade 5 alloy. This indicates, as already



**Fig. 10.** Electron microscopic image of the surface structure of Mo–Nb coating layer (a); images of the structure obtained in characteristic X-ray radiation of Ti (b), Mo (c) and Nb (d) atoms. The arrow in Fig. 10a indicates the coating surface.

**Table 4.** Results of quantitative elemental analysis of the layer of the Mo–Nb coating located at a depth of 10 to 15  $\mu\text{m}$ 

Element	Energy, $E$ , keV	Content		Number of pulses when signal is collected from atoms of given element	Error, %
		wt %	at %		
Al ( $K$ )	1.486	0.31	0.74	2983.89	1.38
Ti ( $K$ )	4.508	44.68	61.47	343966.38	0.01
Nb ( $L$ )	2.166	–	–	–	–
Mo ( $L$ )	2.293	55.01	37.79	135824.56	0.03
Total	–	100	100	–	–

**Fig. 11.** Electron microscopic image of the surface structure of Mo–Nb coating layer prepared by the electroexplosive method: (a) bright field image; (b) microelectron diffraction pattern; (c, d) dark-field images obtained in reflections  $[110]$  Mo (c) and  $[312]$   $\text{Mo}_9\text{Ti}_4 + [112]$   $\text{NbTi}_4$  (d). The arrows in Fig. 11b indicate reflections for (1) dark-field image (c) and (2) dark-field image (d).

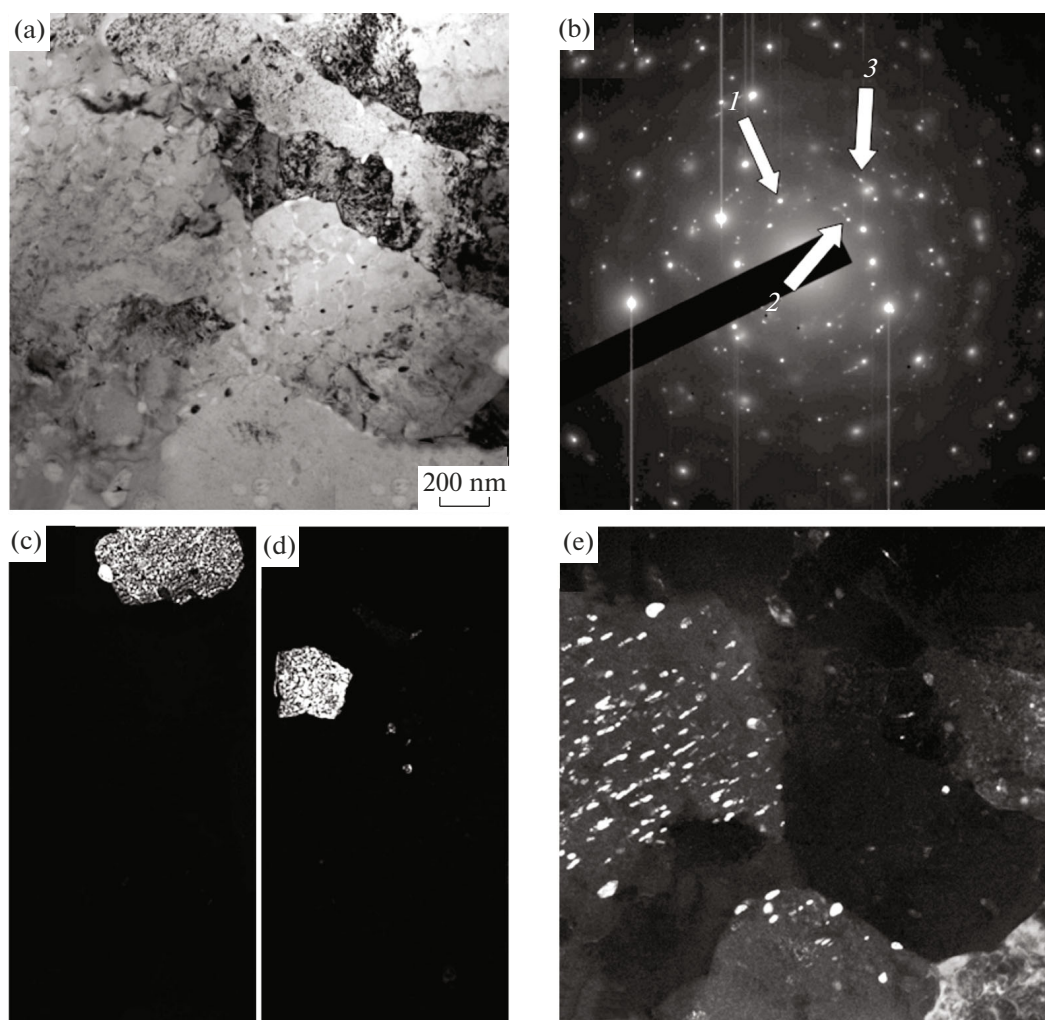


**Fig. 12.** Electron microscopic image of the structure of the layer located at a depth about 8  $\mu\text{m}$ : (a) light-field image; (b) micro-electronogram; (c–e) dark-field images obtained in reflections [100]  $\alpha\text{-Ti}$  (c), [002]  $\alpha\text{-Ti}$  (d), and [200] Nb (e). The arrows in Fig. 11b indicate reflections for (1) dark-field image (c), (2) dark-field image (d), and (3) dark-field image (e).

mentioned above, the mutual diffusion of coating and substrate elements during the electric explosion method. Table 3 presents the elemental composition of the coating surface layer in quantitative terms.

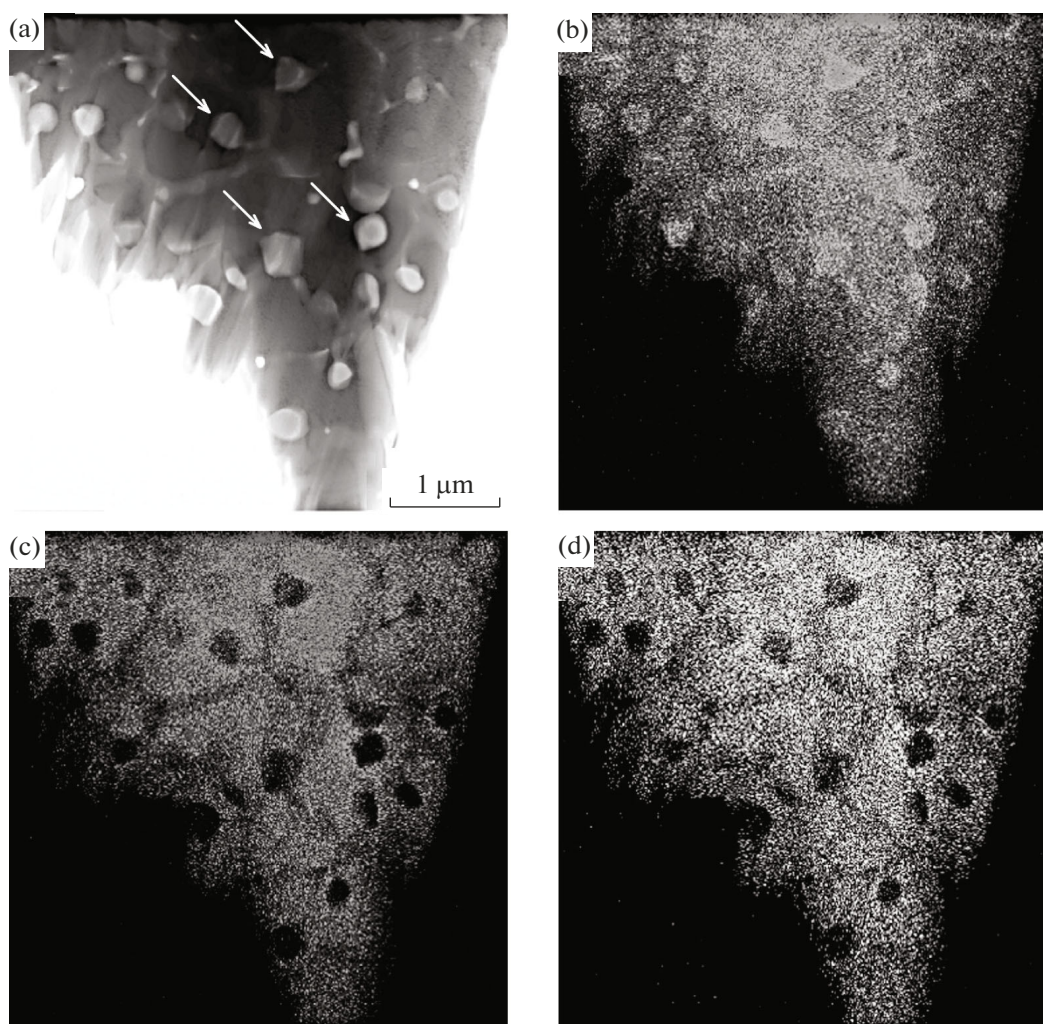
The phase composition of the Mo–Nb coating surface layer was determined by analyzing the microelectron diffraction patterns and corresponding dark-field images (Figs. 11–15).

Figure 11 presents the results of a phase structure analysis of the resulting coating surface layer (coating section 1 in Fig. 10). The major phase of this layer comprises molybdenum grains, while the grain bulk comprises inclusions of the second phase ( $\text{Mo}_9\text{Ti}_4$  and  $\text{NbTi}_4$ ).

Figure 12 shows the results of electron microscopic studies of the structure and phase composition of the

Mo–Nb coating layer located at a depth of about 8  $\mu\text{m}$  (layer 2 in Fig. 10). One can clearly see the presence of titanium and molybdenum grains, as well as niobium particles.

Figure 13 shows the results of elemental analysis of the Mo–Nb coating layer located at a depth of 10 to 15  $\mu\text{m}$ . One can see that its volume is represented by grains enriched in molybdenum and niobium atoms (Figs. 13c and 13d). Inclusions with a high concentration of titanium atoms (Fig. 13b) and sizes ranging from 140 to 230 nm are observed in the volume and along the grain boundaries. Table 4 presents the results of a quantitative analysis of the studied coating layer. The analysis showed that the major elements of this coating layer are titanium and molybdenum. The concentration of titanium atoms in this layer is signifi-



**Fig. 13.** Electron microscopic image of the structure of the Mo–Nb coating layer located at a depth of 10 to 15 mm (a); images of the structure obtained in characteristic X-rays of Ti (b), Mo (c), and Nb (d) atoms.

cantly higher compared to that of the surface layer (Table 3).

Figure 14 presents the structural-phase state of the coating layer located at a depth of 30 to 40  $\mu\text{m}$ , whose analysis showed the presence of two phases. The major phase is a molybdenum-based solid solution (Fig. 14d). Titanium inclusions of various sizes and shapes are located at the boundaries of molybdenum grains (Figs. 14c and 14d).

At a distance of 50  $\mu\text{m}$  from the coating surface, a polycrystalline structure is observed as grains of two dimensional levels: grains with sizes of tens of microns and sizes of 0.5 to 0.7  $\mu\text{m}$  (Fig. 15a) located along the boundaries of larger grains. The microdiffraction analysis showed that the polycrystalline structure of this layer is formed by a solid solution based on  $\alpha$ -Ti, as evidenced by the microelectron diffraction pattern shown in Fig. 15b. At a distance of 70 to 85  $\mu\text{m}$  from

the surface, a polycrystalline structure is already observed, which characterizes Titanium Grade 5 medical alloy in the initial state (Fig. 15c).

The phase composition studies did not reveal any compounds based on vanadium and aluminum, which reduce the biocompatibility of coatings. The detected phases contain only bioinert molybdenum, niobium, and titanium. This allows assuming that the biocompatibility of the resulting coatings will be higher compared to that of Titanium Grade 5 alloy.

#### *Recommendations for Submitting the Resulting Coatings for Clinical Trials of a Specific Type of Implant*

In view of the set of studies carried out on the structure and properties of Mo–Nb coating formed by the electroexplosive method, one can recommend conducting subsequent clinical trials of metal implants

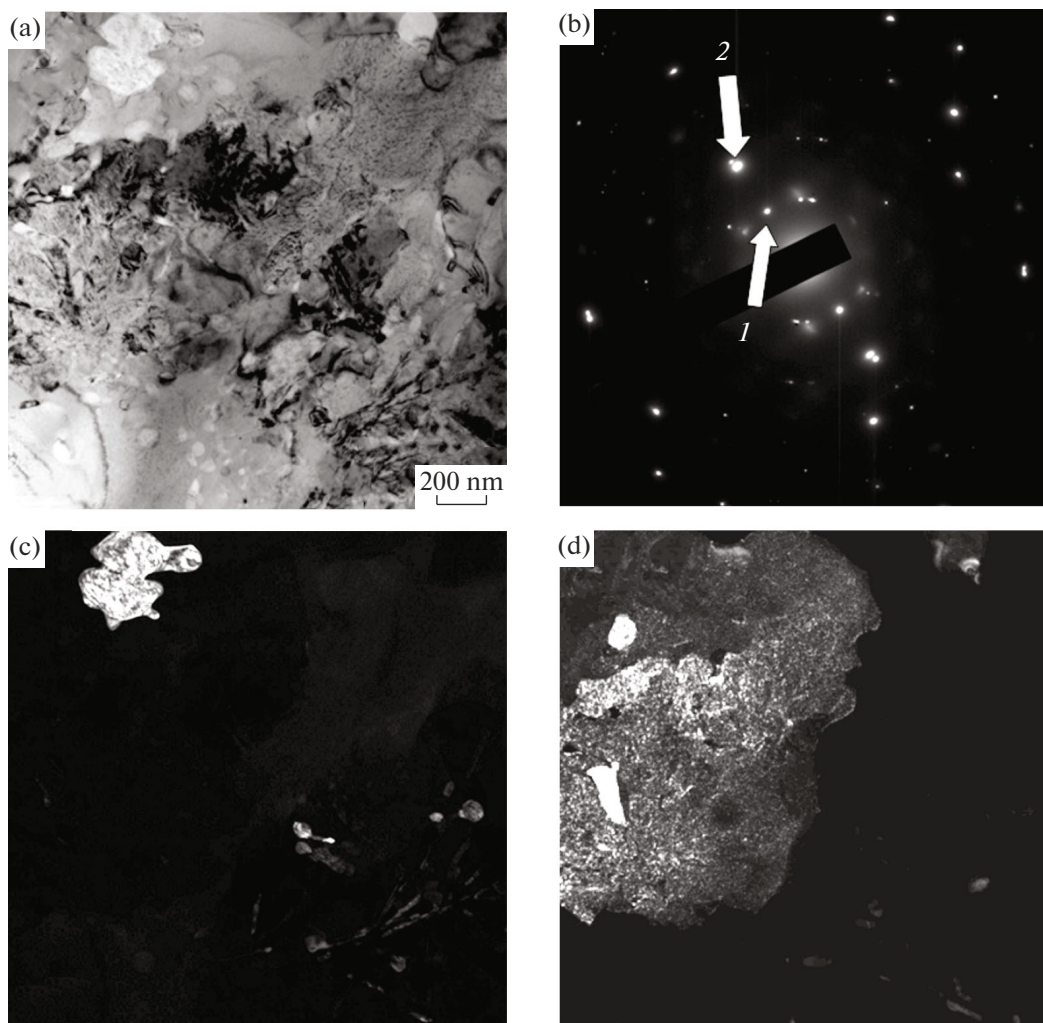


**Fig. 14.** Electron microscopic image of the structure of the layer located at a depth of 30 to 40 mm: (a) light-field image; (b) microelectron diffraction patten; (c, d) dark-field images obtained in reflections  $[100]$   $\alpha$ -Ti (c) and  $[211]$  Mo +  $[201]$   $\alpha$ -Ti (d). The arrows in Fig. 14b indicate reflections for (1) dark-field image (c) and (2) dark-field image (d).

with the resulting coatings, for example, in the case of an elbow joint endoprosthesis, which is used in the treatment of patients with orthopedic injuries and diseases.

## CONCLUSIONS

Thus, studies were carried out on the structure and mechanical properties of a bioinert Mo–Nb coating formed on a substrate made of Titanium Grade 5 medical alloy using the electric explosion method, on the basis of which we can draw the following main conclusions:

(1) The coating surface layer hardness is 60%, and the Young's modulus is 43% higher than the corresponding characteristics of the substrate at a depth of 100  $\mu\text{m}$  and decreases nonmonotonically with distance from the surface. The layer thickness with high

(relative to the substrate) values of hardness and Young's modulus reaches 80  $\mu\text{m}$ .

(2) The wear parameter of the coating surface layer is 1.8-fold greater than that of the substrate. The coating friction coefficient is 1.6-fold higher than that of the substrate.

(3) Along with the coating atoms, the surface layer comprises Al, Ti, and V atoms, thus indicating that the coating is doped with the substrate atoms. The coating stratification by elemental composition was revealed: the top part of the coating is enriched in niobium atoms, and the bottom part is enriched in molybdenum atoms. The coating has a polycrystalline structure formed by a molybdenum-based solid solution. The bulk and the grain boundaries contain inclusions of the second phase comprising  $\alpha$ -Ti, Nb,  $\text{Mo}_9\text{Ti}_4$ , and  $\text{NbTi}_4$  of various shapes and sizes.

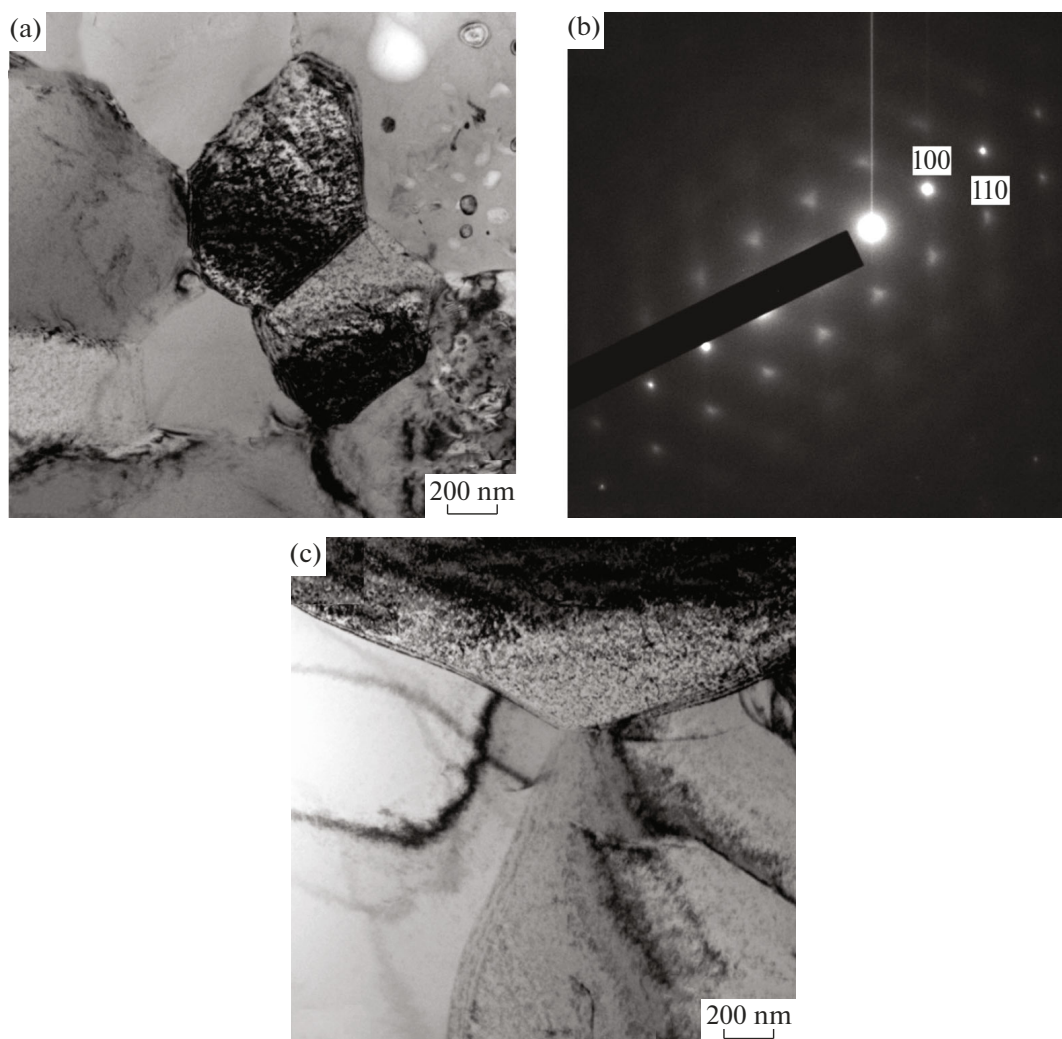


**Fig. 15.** Electron microscopic images of the layer structure located at a depth about 50 mm (a) and 70 to 85 mm (c); (b) micro-electron diffraction pattern of the layer with a depth about 50 mm. The plane of the inverse lattice [001] corresponds to  $\alpha$ -Ti.

(4) In view of the set of the studied structure and properties of the Mo–Nb coating formed by the electric explosion method, the most promising is to conduct subsequent clinical trials of the elbow joint endoprosthesis.

#### FUNDING

This research was funded by the Russian Science Foundation Grant no. 22-79-10012, <https://rscf.ru/project/22-79-10012/>.

#### CONFLICT OF INTEREST

The authors of this work declare that they have no conflicts of interest.

#### REFERENCES

1. Bez, M., Sheyn, D., Tawackoli, W., Avalos, P., Shapiro, G., Giaconi, J.C., Da, X., David, S.B., Gavrity, J., Awad, H.A., Bae, H.W., Ley, E.J., Kremen, T.J., Gazit, Z., Ferrara, K.W., et al., In situ bone tissue engineering via ultrasound-mediated gene delivery to endogenous progenitor cells in mini-pigs, *Sci. Transl. Med.*, 2017, vol. 9, no. 390, p. eaal3128. <https://doi.org/10.1126/scitranslmed.aal3128>
2. Bhumiratana, S., Bernhard, J.C., Alfi, D.M., Yeager, K., Eton, R.E., Bova, J., Shah, F., Gimble, J.M., Lopez, M.J., Eisig, S.B., and Vunjak-Novakovic, G., Tissue-engineered autologous grafts for facial bone reconstruction, *Sci. Transl. Med.*, 2016, vol. 8, p. 343ra83. <https://doi.org/10.1126/scitranslmed.aad5904>
3. Chouirfa, H., Bouloussa, H., Migonney, V., and Falentin-Daudré, C., Review of titanium surface modification techniques and coatings for antibacterial appli-

- cations, *Acta Biomater.*, 2019, vol. 83, pp. 37–54. <https://doi.org/10.1016/j.actbio.2018.10.036>
4. Chen, Q. and Thouas, G.A., Metallic implant biomaterials, *Mater. Sci. Eng., R*, 2015, vol. 87, pp. 1–57. <https://doi.org/10.1016/j.mser.2014.10.001>
  5. Kumari, S., Tiyyagura, H.R., Pottathara, Y.B., Sadasivuni, K.K., Ponnamma, D., Douglas, T.E.L., Skirtach, A.G., and Mohan, M.K., Surface functionalization of chitosan as a coating material for orthopaedic applications: A comprehensive review, *Carbohydr. Polym.*, 2021, vol. 255, p. 117487. <https://doi.org/10.1016/j.carbpol.2020.117487>
  6. Bao, T., Zhou, Z., Gao, P., Dong, X., Chen, J., Zhao, S., Liu, P., and Yin, G., Antibacterial polyelectrolyte coatings enable sustained release of rhBMP-2 from titanium alloy, *Colloid Interface Sci. Commun.*, 2022, vol. 48, p. 100614. <https://doi.org/10.1016/j.colcom.2022.100614>
  7. Khadija, G., Saleem, A., Akhtar, Z., Naqvi, Z., Gull, M., Masood, M., Mukhtar, S., Batool, M., Saleem, N., Rasheed, T., Nizam, N., Ibrahim, A., and Iqbal, F., Short term exposure to titanium, aluminum and vanadium (Ti 6Al 4V) alloy powder drastically affects behavior and antioxidant metabolites in vital organs of male albino mice, *Toxicol. Rep.*, 2018, vol. 5, pp. 765–770. <https://doi.org/10.1016/j.toxrep.2018.06.006>
  8. Costa, B.C., Tokuhara, C.K., Rocha, L.A., Oliveira, R.C., Lisboa-Filho, P.N., and Pessoa, J.C., Vanadium ionic species from degradation of Ti-6Al-4V metallic implants: In vitro cytotoxicity and speciation evaluation, *Mater. Sci. Eng., C*, 2019, vol. 96, pp. 730–739. <https://doi.org/10.1016/j.msec.2018.11.090>
  9. Niinomi, M., Titanium alloys, in *Encyclopedia of Biomedical Engineering*, Narayan, R., Ed., Elsevier Sci., 2019, pp. 213–224. <https://doi.org/10.1016/B978-0-12-801238-3.99864-7>
  10. Oliveira, N.T.C. and Guastaldi, A.C., Electrochemical stability and corrosion resistance of Ti–Mo alloys for biomedical applications, *Acta Biomater.*, 2009, vol. 5, no. 1, pp. 399–405. <https://doi.org/10.1016/j.actbio.2008.07.010>
  11. Ho, W.F., Ju, C.P., and Chern Lin, J.H., Structure and properties of cast binary Ti–Mo alloys, *Biomaterials*, 1999, vol. 20, no. 22, pp. 2115–2122. [https://doi.org/10.1016/s0142-9612\(99\)00114-3](https://doi.org/10.1016/s0142-9612(99)00114-3)
  12. Alves Rezende, M.C.R., Alves, A.P.R., Codaro, E.N., and Dutra, C.A.M., Effect of commercial mouthwashes on the corrosion resistance of Ti-10Mo experimental alloy, *J. Mater. Sci.: Mater. Med.*, 2007, vol. 18, pp. 149–154. <https://doi.org/10.1007/s10856-006-0674-9>
  13. Shokuhfar, T., Hamlekhan, A., Chang, J.Y., Choi, C.K., Sukotjo, C., and Friedrich, C., Biophysical evaluation of cells on nanotubular surfaces: The effects of atomic ordering and chemistry, *Int. J. Nanomed.*, 2014, vol. 9, no. 1, pp. 3737–3748. <https://doi.org/10.2147/IJN.S67344>
  14. Liu, W., Zhan, J., Su, Y., Wu, T., Wu, C., Ramakrishna, S., Mo, X., Al-Deyab, S.S., and El-Newehy, M., Effects of plasma treatment to nanofibers on initial cell adhesion and cell morphology, *Colloids Surf., B*, 2014, vol. 113, pp. 101–106. <https://doi.org/10.1016/j.colsurfb.2013.08.031>
  15. Ishizaki, T., Saito, N., and Takai, O., Correlation of cell adhesive behaviors on superhydrophobic, superhydrophilic, and micropatterned superhydrophobic/superhydrophilic surfaces to their surface chemistry, *Langmuir*, 2010, vol. 26, no. 11, pp. 8147–8154. <https://doi.org/10.1021/la904447c>
  16. Krishnamoorthy, K., Premanathan, M., Veerapandian, M., and Kim, S.J., Nanostructured molybdenum oxide-based antibacterial paint: Effective growth inhibition of various pathogenic bacteria, *Nanotechnology*, 2014, vol. 25, no. 31, p. 315101. <https://doi.org/10.1088/0957-4484/25/31/315101>
  17. Qureshi, N., Patil, R., Shinde, M., Umarji, G., Causin, V., Gade, W., Mulik, U., Bhalerao, A., and Amalnerkar, D.P., Innovative biofilm inhibition and anti-microbial behavior of molybdenum sulfide nanostructures generated by microwave-assisted solvothermal route, *Appl. Nanosci.*, 2015, vol. 5, pp. 331–341. <https://doi.org/10.1007/s13204-014-0322-5>
  18. Krishnamoorthy, K., Premanathan, M., Veerapandian, M., and Kim, S.J., Nanostructured molybdenum oxide-based antibacterial paint: Effective growth inhibition of various pathogenic bacteria, *Nanotechnology*, 2014, vol. 25, no. 31, p. 315101. <https://doi.org/10.1088/0957-4484/25/31/315101>
  19. Krishnamoorthy, K., Premanathan, M., Veerapandian, M., and Kim, S.J., New function of molybdenum trioxide nanoplates: Toxicity towards pathogenic bacteria through membrane stress, *Colloids Surf., B*, 2013, vol. 112, pp. 521–524. <https://doi.org/10.1016/j.colsurfb.2013.08.026>
  20. Ali, A.M., Thair, L., and Intisar, J., Studying biomimetic coated niobium as an alternative dental implant material to titanium (*in vitro* and *in vivo* study), *Baghdad Sci. J.*, 2018, vol. 15, no. 3, pp. 253–261. <https://doi.org/10.21123/bsj.2018.15.3.0253>
  21. Achache, S., Lamri, S., Arab Pour Yazdi, M., Billard, A., François, M., and Sanchette, F., Ni-free superelastic binary Ti–Nb coatings obtained by DC magnetron co-sputtering, *Surf. Coat. Technol.*, 2015, vol. 275, pp. 283–288. <https://doi.org/10.1016/j.surfcoat.2015.05.005>
  22. Lyasnikov, V.N., Lyasnikova, A.V., and Dudareva, O.A., *Plazmennoe napylenie* (Plasma Spraying), Saratov: Gagarin Saratov State Tech. Univ., 2016.
  23. Perinskaya, I.V., Perinsky, V.V., Rodionov, I.V., and Kuts, L.E., Additive ion implantation in gallium arsenide by forming alloy nanoclusters, *Inorg. Mater.: Appl. Res.*, 2023, vol. 14, pp. 604–609. <https://doi.org/10.1134/S2075113323030334>
  24. Perinskii, V.V. and Perinskaya, I.V., *Additivnaya implantatsiya ionov v perekhodnye metally, poluprovodniki, dielektriki tonkoplenochnykh struktur: Monografiya* (Additive Ion Implantation into Transition Metals, Semiconductors, and Thin Film Dielectrics: Monograph),

Moscow: IPR Media, 2022.

<https://doi.org/10.23682/116611>

25. Romanov, D.A., Sosnin, K.V., Gromov, V.E., Bataev, V.A., Ivanov, Yu.F., Glezer, A.M., and Sundeev, R.V., Titanium-zirconium coatings formed on the titanium implant surface by the electroexplosive method, *Mater. Lett.*, 2019, vol. 242, pp. 79–82.

<https://doi.org/10.1016/j.matlet.2019.01.088>

26. Han, F., Zhu, L., Liu, Z., and Gong, L., The study of refractory Ta10W and non-refractory Ni60A coatings deposited by wire electrical explosion spraying, *Surf.*

*Coat. Technol.*, 2019, vol. 374, pp. 44–51.

<https://doi.org/10.1016/j.surfcoat.2019.05.065>

27. Tarasov, S.Yu., Polyakov, S.N., and Bikbaev, S.A., Visualization of localized deformation in friction *Fiz. Mezhomekh.*, 2005, vol. 8, no. 2, pp. 93–98.

*Translated by A. Pisarevskii*

**Publisher's Note.** Pleiades Publishing remains neutral with regard to jurisdictional claims in published maps and institutional affiliations.